2011 American Control Conference
on O'Farrell Street, San Francisco, CA, USA
June 29 - July 01, 2011

# Hybrid Electric Vehicle Supervisory Control Design Reflecting Estimated Lithium-Ion Battery Electrochemical Dynamics

Tae-Kyung Lee, Youngki Kim, Anna Stefanopoulou, and Zoran S. Filipi

*Abstract*—**Accurate prediction of the battery electrochemical dynamics is important to avoid undesired battery operation under aggressive driving. This paper proposes a battery power management strategy considering Li-ion concentration in the electrodes to prevent excessive battery charging and discharging. The proposed approach adjusts the allowable battery power limits through the feedback of the estimated electrode-averaged Li-ion concentration information. An advanced hybrid electric vehicle (HEV) power split strategy is constructed implementing a Li-ion battery model with electrochemical diffusion dynamics to capture the battery dynamic behavior under transients. A novel contribution arises from the implementation of an extended Kalman filter (EKF) using uneven discretization of the particle radius for fast and accurate prediction of the Lithium intercalation dynamics. The control design modifies the allowable battery power limit used in the supervisory controller, thus, maintaining low complexity of the control structure.**

## I. Introduction

CONTROL design of hybrid electric vehicle (HEV) or plug-in HEV (PHEV) is important to obtain the maximum hardware potential and to prevent battery degradation. The supervisory control affects battery operations regardless of HEV configurations: series HEV, parallel HEV, and power-split HEV. In the series HEV, propulsion power is entirely dependent on electric power, and the electric power is only delivered by the battery and the generator. Thus, supervisory controller must manage the electricity requirement for each electric component to achieve the desired performance and to prevent the possible abnormal operations. The current levels are generally high. Recently, Lithium-ion (Li-ion) batteries have been used in the electric vehicle (EV) and (P)HEV due to its high energy density. However, Li-ion battery is less durable than other types of rechargeable batteries, such as nickel metal hydride or nickel-cadmium designs. Thus, preventing overcharging and discharging is critical for improving the battery life and stability.

Electrochemical models of the Li-ion battery were developed by Doyle et al. [1], and further improved in the following studies [2],[3]. The full order electrochemical models can predict the solid concentration profiles across the electrodes and electrolyte, but, their long computational time and the extensive model complexity prevent their application in control design and real-time on-board estimator. Reduced battery models are beneficial for model-based battery control design. To reduce the model order for fast simulation, a residue grouping approach was proposed by Smith *et al*. [4],[5]. The approach showed good prediction accuracy, yet the Li-ion diffusion dynamics toward the center of the solid particle is not observable in this model. Another approach is the model reduction using the simple electrode-averaged, single-particle model proposed by Di Domenico *et al.* [6], [7]. The averaged model is valid when the concentration distribution along the length of the electrodes and separator can be assumed constant. Regardless of the limitation, the averaged model provides Li-ion concentration profiles in the electrodes and can produce a state-space system with linear dynamics of spherical diffusion in the solid material and a nonlinear voltage output equation [6],[7]. Thus, the averaged battery model is used for prediction of Li concentration via a Kalman filter design with measured terminal voltage and applied current.

Many previous simulation-based HEV studies and design optimizations used equivalent circuit battery models. In those cases, fuel economy and battery operation are executed without the consideration of electrochemical diffusion dynamics [8], [9]. The terminal voltage is directly affected by the solid-electrolyte concentration, and high discharge rate results in sudden voltage drops and Li-ion depletion at the boundary of the electrolyte with the solid particles [6],[7]. Such effects become more important in predicting battery behavior under transients.

In the present paper, a control strategy with the consideration of the Li-ion diffusion dynamics is proposed to moderate excessive battery charging and discharging. The proposed control design is devised to utilize the predicted dynamics without excessive increase of the control structure complexity by augmenting the rule-based supervisory controller. It modifies the allowable battery power for the supervisory controller. First, we propose a HEV simulation framework to design supervisory control including the electrode-averaged Li-ion battery model. Then, model-driven extended Kalman filter (EKF) is designed and is implemented to estimate the Li-ion concentration in a representative solid particle. A controller for compensating the battery power limits is designed using the estimated Li-ion concentration profile. Then, the effects of the proposed controller on battery

Tae-Kyung Lee is with the University of Michigan, Ann Arbor, MI 48109, USA (kteel@umich.edu).

Youngki Kim is with the University of Michigan, Ann Arbor, MI 48109, USA (youngki@umich.edu).

Anna Stefanopoulou is with the University of Michigan, Ann Arbor, MI 48109, (annastef@umich.edu).

Zoran S. Filipi is with the University of Michigan, Ann Arbor, MI 48109 USA (corresponding author, phone: 734-936-0427; fax: 734-764-4256; e-mail: filipi@umich.edu).

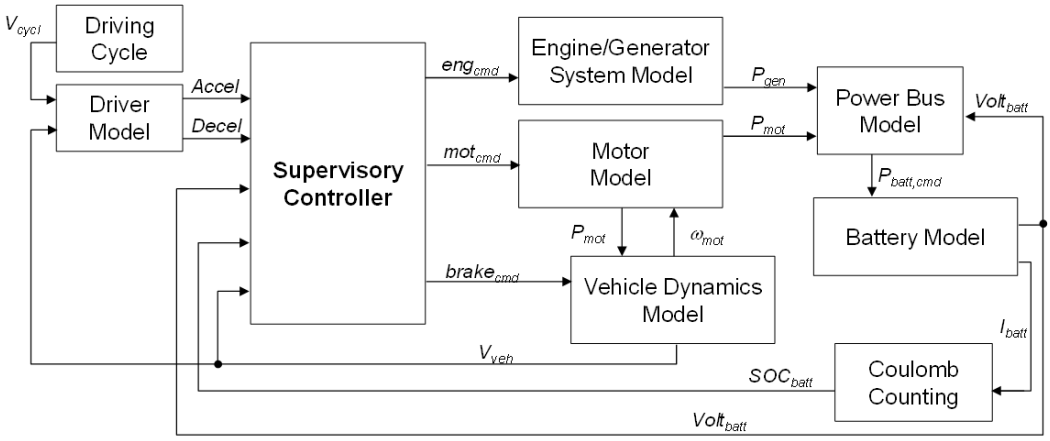


Fig. 1. Simulation frame work of the series hybrid electric vehicle in SIMULINK with a forward-looking approach

responses are reviewed, and this paper is summarized with conclusions.

## II. Simulation Framework for Control Design

HEV simulation framework is constructed to obtain realistic responses of each component with the balance of computation time and prediction accuracy. A heavy-duty series HEV equipped with a relatively small battery is selected as the target vehicle to investigate the effect of the electrochemistry battery dynamics on control design. The heavy-duty series HEV requires high propulsion power due to the large mass. The propulsion power entirely comes from electricity. Table 1 shows the specification of the target vehicle and battery size. The component sizes were initially determined to satisfy the performance targets: maximum speed, gradeability, and acceleration. Rolling resistance, drag, and grade terms are taken into account in the vehicle power demand.

$$m_e \dot{v}_{veh} = F_{prop} - F_{RR} - F_{WR} - F_{GR}, \quad (1)$$

where $F_{net}$ is the net force applied to the vehicle, $F_{prop}$ is the propulsion force from the powertrain, $F_{RR}$ is the rolling resistance force, $F_{WR}$ is the wind resistance force, $F_{GR}$ is the grade resistance force and all other external forces applied to the vehicle, $m_e$ is the equivalent vehicle mass, $v_{veh}$ is the vehicle velocity, and $a_{veh}$ is the vehicle acceleration.

Figure 1 shows the overall vehicle simulation framework. The vehicle model is a forward looking model, and the driver determines control commands to follow desired velocity profiles. The supervisory controller assigns propulsion and braking power to the engine and the motor respectively. Then, the electric power demand to the battery is determined as

$$P_{batt} = -P_{egn} + P_{mot} + P_{accs}, \quad (2)$$

where $P_{batt}$ is the battery output power, $P_{mot}$ is the motor output power, $P_{eng}$ is the engine output power, and $P_{accs}$ is electric accessory power. The required $P_{batt}$ determines the current input to the battery, $I_{batt}$, using the battery terminal voltage, $V_{batt}$, and the terminal voltage is calculated from the finely discretized averaged electrochemistry battery model. We note that the only input to the battery cell model is "current", and the only output to the battery cell is "terminal voltage" in the simulation framework same as in a real vehicle.

TABLE I
Heavy-duty Series-HEV Specification: Hybridized M-ATV

| | Specification |
|---|---|
| Vehicle | Hybridized M-ATV |
| Weight | 13,400 kg |
| Payload | 1,814 kg (4000 lbs) |
| Frontal area | 5.72 $m^2$ (Width/Height: 2.49/2.70 m) |
| Engine | I6 Turbo-diesel engine: 275 kW |
| Generator | Permanent Magnet: 275 kW |
| Battery | Li-ion 6.0 kWh |
| Motors | Permanent Magnet: 380kW |

## III. Electrode-Averaged Battery Model

Li-ion battery cells are modeled by describing the key dynamics of charging and discharging in the electrodes. In the averaged electrochemistry model, Li-ion concentration change in the solid particles along the electrode is neglected, and the concentration in the electrolyte concentration is assumed as constant. Although the simplification may lose the prediction accuracy under high charging and discharging conditions, important diffusion dynamics in the solid particle are captured.

Figure 2 (a) shows the general structure of Li-ion batteries, and it consists of three parts: two porous electrodes, cathode and anode, and a separator between those two electrodes. The potential energy difference in each electrode generates voltage. Li-ions have the lowest potential energy in the interstitial sites within the solid crystalline structure of the cathode. During the charging process, Li-ions are forced to move from the cathode to the anode. The Li-ions diffuse to the surface within the cathode's solid structure, then, traveling through the electrolyte across the separator, and entering into the anode. During the discharging process, the Li-ions diffuse into the anode's interstitial sites.

The key equations presented by Di Domenico et al. [6],[7] for the averaged electrochemistry battery model (see- Fig. 2 (b)) are derived from the complete set of equations describing the Li-ion battery system with solid and electrolyte concentrations ($c_s$, $c_e$) and solid and electrolyte potentials ($\phi_s$, $\phi_e$) by Fuller *et al.*[2],

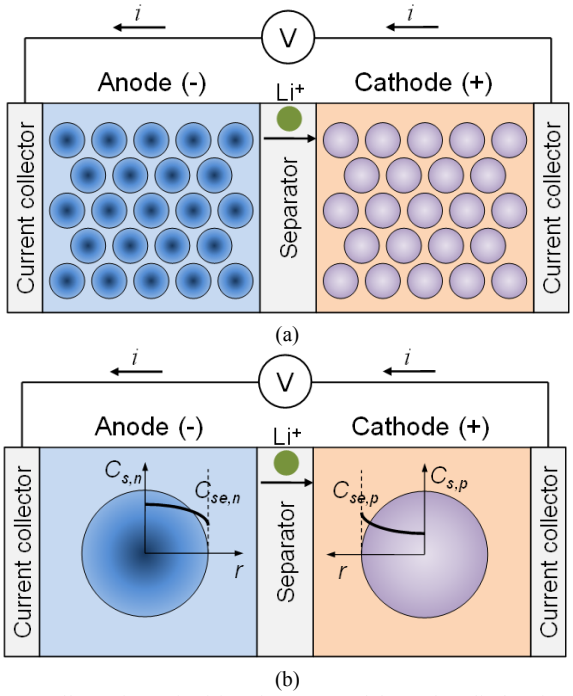


Fig. 2. Illustration of Li-ion battery models under discharging: (a) macroscopic (x-direction) cell model with coupled microscopic solid diffusion model (r-direction), (b) electro-averaged cell model with coupled microscopic solid diffusion model (r-direction)

$$\vec{\nabla}_x \kappa^{eff} \vec{\nabla}_x \phi_e = -j^{Li}, \tag{3}$$

$$\vec{\nabla}_x \sigma^{eff} \vec{\nabla}_x \phi_s = j^{Li}, \tag{4}$$

$$\frac{\partial \varepsilon_e c_e}{\partial t} = \vec{\nabla}_x \left( D_e^{eff} \vec{\nabla}_x c_e \right) + \frac{1-t^0}{F} j^{Li}, \tag{5}$$

$$\frac{\partial c_s}{\partial t} = \vec{\nabla}_r \left( D_s \vec{\nabla}_r c_s \right), \tag{6}$$

where $\kappa^{eff}$ is the effective electrolyte phase conductivity, $\sigma^{eff}$ is the effective solid phase conductivity, $F$ is the Faraday's constant, $D_e^{eff}$ and $D_s$ are the effective diffusion coefficient of Li-ion in the electrolyte and electrodes respectively, $t^0$ is the transfer number of the Li-ion with respect to the velocity of solvent, and $j^{Li}$ is the Butler-Volmer current density defined as

$$j^{Li} = a_s j_0 \left[ \exp\left( \frac{\alpha_a F}{RT} \eta \right) - \exp\left( -\frac{\alpha_c F}{RT} \eta \right) \right], \tag{7}$$

where $a_s$ is the active surface area per electrode unit volume, $\alpha_a$ and $\alpha_c$ are the anodic and cathodic transfer coefficients of electrode, $R$ is the universal gas constant, $T$ is the absolute temperature, and $\eta$ is an over-potential obtained as

$$\eta = \phi_s - \phi_e - U(c_{se}), \tag{8}$$

where $c$ is the volume-averaged Li-ion concentration with subscripts $e$ and $s$ referring to the concentration in the electrolyte and solid phases, $U(c_{se})$ is the open circuit potential and expressed by empirical correlation function of the solid surface concentration, $c_{se}$, which is the electrode-average solid concentration at the electrolyte interface, and $j_0$ is the exchange current density dependent on the solid and electrolyte concentration,

$$j_0 = k (c_e)^{\alpha_a} \left( c_{s,\max} - c_{se} \right)^{\alpha_a} (c_{se})^{\alpha_c}. \tag{9}$$

The terminal voltage is computed as

$$V = \phi_s (x = L) - \phi_s (x = 0) - \frac{R_f}{A} I, \tag{10}$$

where $R_f$ is the film resistance on the electrode surface, and $A$ is the collectors surface, and $I$ is the applied current.

In an averaged electrochemistry model represented by one solid particle for each electrode (anode and cathode), the Butler-Volmer current is assumed constant $\bar{j}_n^{Li}$ regardless spatial locations, and it is evaluated from the spatial integral.

$$\bar{j}^{Li} = \frac{1}{\delta} \frac{I}{A} = \frac{1}{\delta} \int_0^{\delta} j^{Li}(x) dx, \tag{11}$$

where $\delta$ is the electrode thickness.

The model is then expressed as a set of ordinary differential equations (ODE) by using the finite difference method for the spatial variable $r$ so that it is used as the battery control oriented model. The sphere radius is divided into $\boldsymbol{r} = (r_1, r_2, \ldots, r_{Mr-1})$ with uneven discretization. The system states are distributed Li-ion concentration in the solid, $\boldsymbol{c_s} = (c_{s,1}, c_{s,2}, \ldots, c_{s,Mr-1})^{\mathrm{T}}$. The resulting state-space equation is expressed as

$$\dot{\boldsymbol{c}}_{\boldsymbol{s}} = \boldsymbol{A}\boldsymbol{c}_{\boldsymbol{s}} + \boldsymbol{B}u, \tag{12}$$

where $\boldsymbol{A}$ is a constant tri-diagonal matrix determined from

$$\dot{c}_{s,k} = \frac{2D_s}{\Delta r_{k-1} + \Delta r_k} \left[ \left( \frac{1}{\Delta r_{k-1}} - \frac{1}{r_k} \right) c_{s,k-1} - \left( \frac{1}{\Delta r_k} + \frac{1}{\Delta r_{k-1}} \right) c_{s,k} + \left( \frac{1}{\Delta r_k} + \frac{1}{r_k} \right) c_{s,k+1} \right], \tag{13}$$

for $k$=2, …$Mr$–2, and $\Delta r_k = r_{k+1} - r_k$, with boundary conditions:

$\left. \frac{\partial c_s}{\partial r} \right|_{r=0} = 0$ resulting in $c_{s,0} = c_{s,1}$ at the center ($k$=1), and

$\left. \frac{\partial c_s}{\partial r} \right|_{r=R_s} = -\frac{\bar{j}^{Li}}{F a_s D_s}$ resulting in

$c_{se} = c_{s,Mr} = c_{s,Mr-1} - \Delta r_{Mr-1} \frac{\bar{j}^{Li}}{F a_s D_s}$ at the solid particle surface.

The battery voltage (8), using the average values at the anode and the cathode, can be written as

$$V = \left( \bar{\eta}_p - \bar{\eta}_n \right) + \left( \bar{\phi}_{e,p} - \bar{\phi}_{e,n} \right) + \left( U_p(\theta_p) - U_n(\theta_n) \right) - \frac{R_f}{A} I. \tag{14}$$

where $\theta = c_{se} / c_{s,\max}$ is normalized solid-electrolyte concentration, and $\bar{\eta}_p - \bar{\eta}_n$ can be expressed as

$$\bar{\eta}_p - \bar{\eta}_n = \frac{RT}{\alpha_a F} \ln \frac{\xi_p + \sqrt{\xi_p^2 + 1}}{\xi_n + \sqrt{\xi_n^2 + 1}}, \quad (15)$$

from the equations (7) and (8),

where $\xi_p = \frac{\bar{j}_p^{Li}}{2a_s j_{o,p}}$ and $\xi_n = \frac{\bar{j}_n^{Li}}{2a_s j_{o,n}}$, and

$$\bar{\phi}_{e,p} - \bar{\phi}_{e,n} = \phi_e(L) - \phi_e(0) = -\frac{I}{2Ak^{eff}}(\delta_n + 2\delta_{sep} + \delta_p). \quad (16)$$

where $\delta$ is the electrode thickness with subscripts $p$, $sep$, and $n$ referring to the cathode, the separator, and the anode. Finally, the battery voltage (12) can be written as a function of current demand and average solid concentration,

$$V = \frac{RT}{\alpha_a F} \ln \frac{\xi_p + \sqrt{\xi_p^2 + 1}}{\xi_n + \sqrt{\xi_n^2 + 1}} + \left(U_p(\theta_p) - U_n(\theta_n)\right) - \frac{K_r}{A} I, \quad (17)$$

where $K_r = \frac{I}{2Ak^{eff}}(\delta_n + 2\delta_{sep} + \delta_p) + R_f$ is a term accounting for both internal and collector film resistances, $k^{eff}$ is the effective electrolyte phase conductivity.

## IV. Supervisory Control Design

The supervisory controller is designed by augmenting the thermostatic SOC control strategy with additional logic for limiting potentially harmful charging/discharging power. The controller consists of four driving modes, and it distributes the required propulsion power between the engine and the battery depending on either SOC (energy), or demanded rates of charging/discharging (power). The modes and rules are summarized as follows:

*(1)* Electric mode

if $0 < P_{dem} < P_{batt.max}$ and $SOC_{batt} > SOC_{ub}$,
$P_{mot} = P_{dem}$, $P_{eng} = 0$, $P_{batt} = P_{mot} + P_{accs}$.

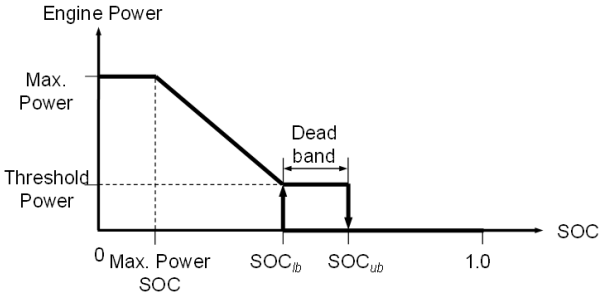


Fig. 3. Illustration of the thermostatic SOC power management control

*(2)* Thermostatic control mode

if $0 < P_{dem} < P_{batt.max}$ and $SOC_{batt} < SOC_{ub}$,
$P_{mot} = P_{dem}$, $P_{eng} = f(SOC_{batt})$ in Fig. 3,
$P_{batt} = -P_{eng} + P_{mot} + P_{accs}$.

*(3)* Power mode

if $P_{dem} > P_{batt.max}$,
$P_{mot} = P_{dem}$, $P_{eng} = P_{mot} + P_{accs} - P_{batt.max}$,
$P_{batt} = P_{batt.max}$.

*(4)* Braking mode

if $P_{batt.min} < P_{dem} < 0$,
$P_{mot} = P_{dem}$, $P_{eng} = 0$, $P_{batt} = P_{mot} + P_{accs}$,
else if $P_{dem} < P_{batt.min}$,
$P_{mot} = P_{batt.min}$, $P_{eng} = 0$, $P_{mech.brk} = P_{dem} - P_{mot}$,
$P_{batt} = P_{mot} + P_{accs}$.

The thermostatic SOC control strategy has been used in series hybrid hydraulic vehicle (HHV) and HEV control design in several previous studies [8],[10]. It is very effective in managing SOC, and providing efficiency gains when combined with optimal engine operating scheme [10]. The basics of the thermostatic SOC control are illustrated in Fig. 3. Whenever the battery SOC hits the lower limit denoted on $SOC_{lb}$ in Fig. 3, the engine begins charging the battery with the threshold power until the battery SOC reaches to the

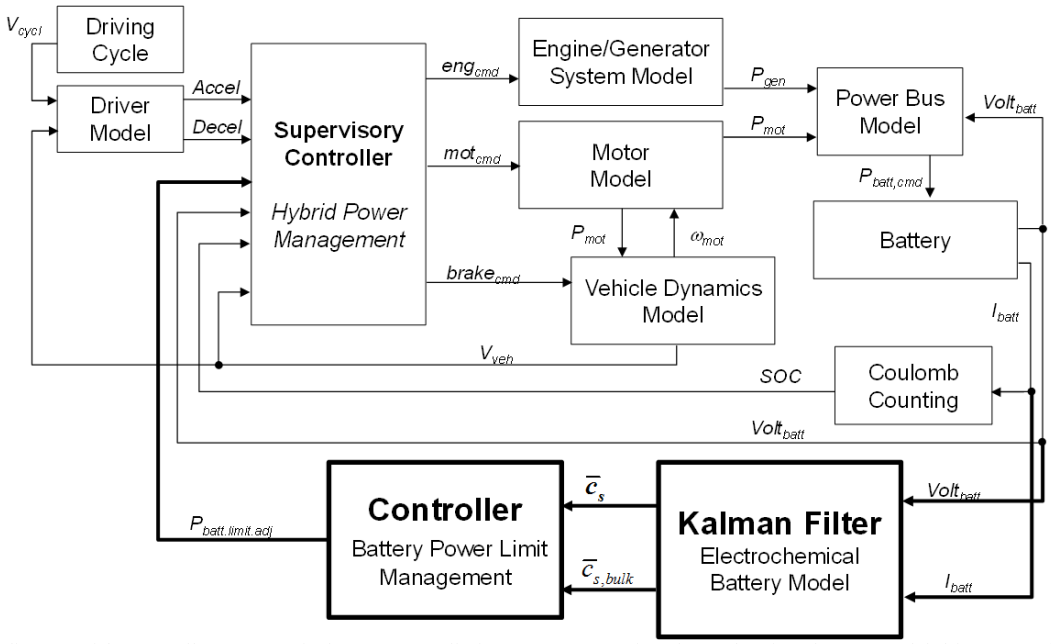


Fig. 4. Schematic diagram of the controller structure for battery power limits management using electrochemistry battery model-driven extended Kalman filter

$SOC_{ub}$. When the battery SOC is lower than the $SOC_{lb}$, the engine power demand is determined depending on the current SOC as shown in Fig. 3, and threshold power. The engine power is delivered with a combination of torque-speed that keeps the engine operated on the best *bsfc* (brake specific fuel consumption) line for the minimum fuel consumption [8].

We propose to augment this by monitoring the instantaneous battery power, and triggering the Mode 3 whenever the power reaches potentially harmful levels. The allowable battery power limits ($P_{batt,max}$ and $P_{batt,min}$) prevent battery over-charging and over-discharging, and the Mode 3 rule adds a new layer to the supervisory controller. The key to the successful implementation is prediction of allowable battery power limits using estimated instantaneous Li-ion concentration by the electrochemical model-driven extended Kalman filter (EKF). The schematic diagram of the controller structure is shown in Fig. 4. The allowable battery power limits are adjusted by the Mode 3 controller and fed into the supervisory controller. Then, the supervisory controller distributes the demanding power to the engine and battery using the rules.

High current discharging causes a sudden Li-ion concentration change at the surface of the solid material, thus, resulting in sudden voltage drops. Terminal voltage of the battery is sensitive to both the SOC and Li-ion solid surface concentration. In contrast, high current charging causes a sudden voltage rise. If the battery power demand is determined without the consideration of the battery diffusion dynamics, the battery could be over-charged and over-discharged under severe acceleration and braking respectively. It can be explained as follow: when the solid surface concentration is changed suddenly under discharging, the available power is significantly lowered although the SOC remains almost same. If the controller has no information of the battery internal states, it determines battery power demand based only on the SOC and terminal voltage. Thus, the required power exceeds the battery capability, and the battery could be eventually damaged. The proposed strategy is actively engaged to prohibit it.

### *A. Model-driven Extended Kalman Filter*

The electrode-averaged model based EKF design proposed by Di Domenico et al. [7] is used as a battery state estimator. The model is expressed as

$$\begin{aligned} \dot{\hat{\boldsymbol{x}}} &= \boldsymbol{A}_p \hat{\boldsymbol{x}} + \boldsymbol{B}_p u + K_e (y - \hat{y}) \\ \hat{y} &= V(\hat{x}, u) \end{aligned} \quad , \qquad (18)$$

where $\hat{\boldsymbol{x}}$ and $\hat{y}$ are the estimate state $\boldsymbol{x}$ and output $\boldsymbol{y}$. The state $\hat{\boldsymbol{x}} = (\hat{c}_{s,p1}, \hat{c}_{s,p2}, \ldots, \hat{c}_{s,p(Mr-1)})^T$. The matrices $\boldsymbol{A_p}$ and $\boldsymbol{B_p}$ are obtained from eqn. (12). The nonlinear output is linearized by $C=\partial V/\partial x$, which is a row matrix with zeros in its first $Mr-2$ elements. The last non-zero term is numerically computed from $\partial V / \partial \hat{c}_{s,p(Mr-1)}$ in the EKF.

To reduce the computation efforts while maintaining the estimation accuracy, the solid radius is discretized with a small number of uneven steps after reviewing the Li-ion concentration profiles under various operations. The number of states is set to eight (8), and the estimated states are compared to the reference battery model with 49 states for the

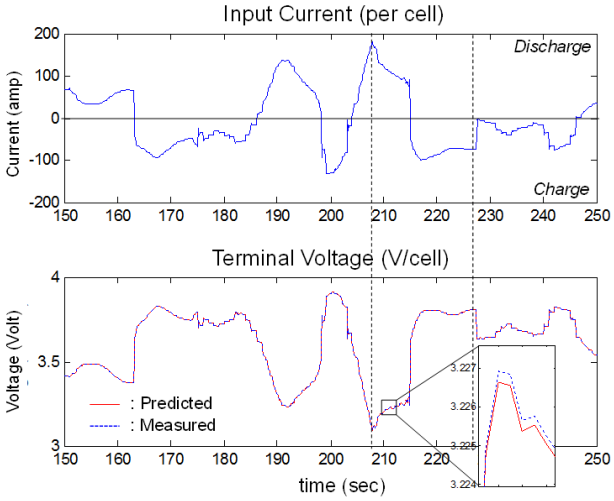


Fig. 5. Transient response of the terminal voltage predicted from the extended Kalman filter and measured from the 98th order electrode-averaged battery model

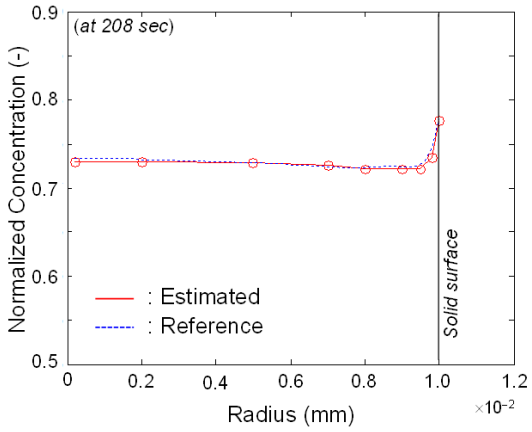


(a)

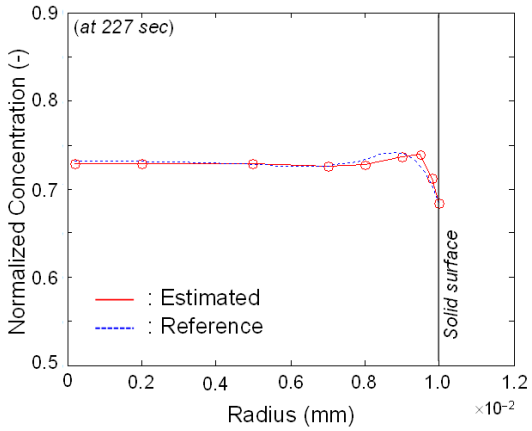


(b)

Fig. 6. Comparison between estimated and reference Li-ion concentrations under fast transient: (a) discharging; (b) charging

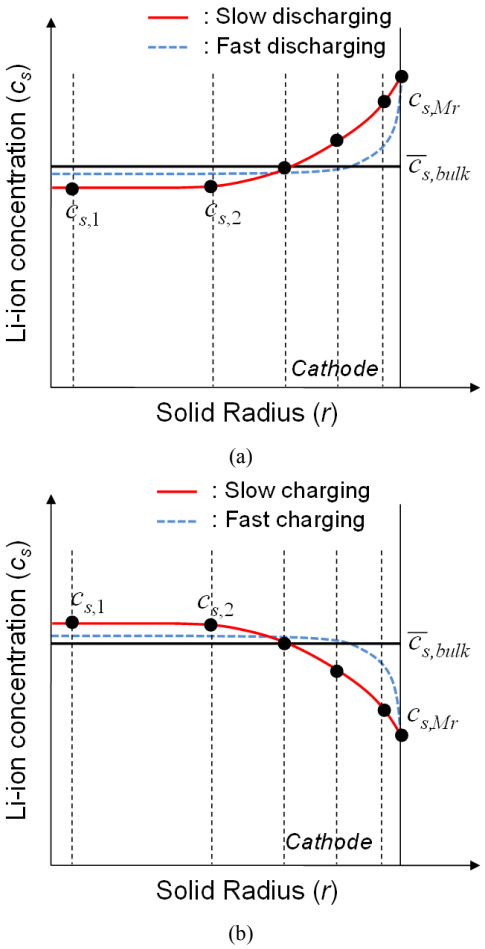


Fig. 7. Illustration of Li-ion concentration at the cathode under the different magnitudes: (a) discharging; (b) charging

Li-ion concentration in the cathode.

The Kalman gain is obtained by

$$K_e = PCR^{-1}, \tag{19}$$

where $P$ is the solution of the Ricatti equation

$$\begin{aligned} \dot{P} &= A_p P + PA_p^T - PCR^{-1}C^T P + Q \\ P(0) &= P_0 \end{aligned}, \tag{20}$$

and $Q$ and $R$ are positive definite matrices to obtain small battery voltage prediction errors. While solving the Ricatti equation, the P matrix is reinitialized whenever the battery current direction is changed. Furthermore, $\partial V / \partial \hat{c}_{s,p(Mr-1)}$ frequently has a large number under transient, thus, resulting in abnormally large Kalman gains and causing large estimation errors. Thus, the ranges of $P$ and $K_e$ are limited to avoid the high estimation errors of Li-ion concentration, and the designed filter is capable of estimating the Li-ion concentration with sufficient accuracy over the entire battery operating range.

The voltage outputs from the EKF and the reference battery model under fast transient are shown in Fig. 5. The accurate tracking performance validates the proposed approach to obtain the appropriate Kalman gains. Estimation results under severe transients (up to 30C) are presented at both charging and discharging. The reference concentrations are obtained from the high order averaged electrochemistry Li-ion battery model. We note that sudden discharging significantly changes the Li-ion concentration near the solid boundary (-see Fig. 6 (a)), although concentrations deeper inside the particle solid are almost constant. Figure 6 (b) also shows that the concentration profile has multiple curvatures along the particle radius under sequential charging and discharging events or vice versa.

### B. *Battery Power Management Strategy*

The adjustment amount of the battery power limits is determined using the Li-ion concentration along the solid radius direction and the averaged Li-ion concentration computed from the bulk SOC. Figure 7 illustrates the concentration change with different discharging current with the same SOC calculated by coulomb counting and the same solid surface concentration. Despite the similar SOC, bulk Li-ion concentration, $\overline{c}_{s,bulk}$, and the solid surface concentration, the available discharging current, which is defined as the maximum discharging current dropping the terminal voltage to the lower voltage limit, could be different. The relaxation time of the concentration of the fast discharging case is shorter than the slow discharging case with the same SOC and the surface concentration. Thus, not only the Li-ion concentration at the solid surface but also the entire Li-ion concentration profile must be considered by the battery management control design.

The control command for the modification of the allowable battery power limits is computed through the proportional-integral (PI) feedback of the following cost function,

$$J = \sum_{i=1}^{M_r-1} w_i (\overline{c}_{s,bulk} - \hat{c}_{si}), \tag{21}$$

where $\overline{c}_{s,bulk}$ is the averaged Li-ion concentration, $\hat{c}_{si}$ is the estimated Li-ion concentration at the $i$th radial segment of solid, $w_i$ is the weighting at the $i$th element. The weighting vector $\boldsymbol{w} = (w_1, w_2, \ldots, w_{Mr-1})$ is tuned to capture the effect of the concentration profile on the battery available power limit, and higher weights are assigned near the solid surface.

## V. Simulation Results

Performance of the supervisory control design is investigated through HEV simulation. To emphasize the controller performance, aggressive military driving cycles, "*urban assault cycle*" (-see Fig. 8), and a relatively small battery (6 kWh) is used for the heavy vehicle (13.4 ton). The battery capacity per cell is 6AH and the nominal voltage is 3.6 V. The resulting maximum available power from battery is marginal to propel the vehicle under the cycle, thus, accurate control is required to prevent battery over-charging and over -discharging.

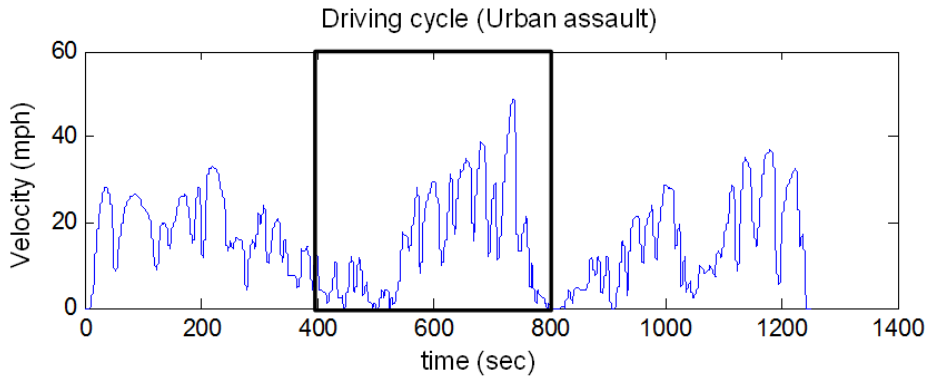


Fig. 8. Urban assault driving cycle velocity profile

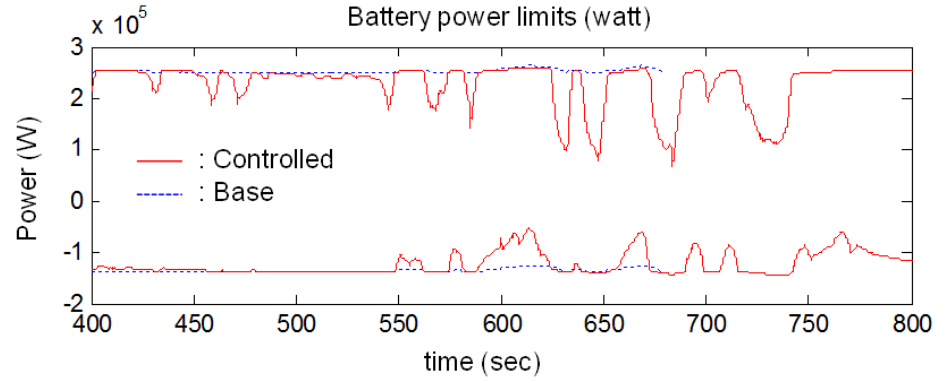


(a)

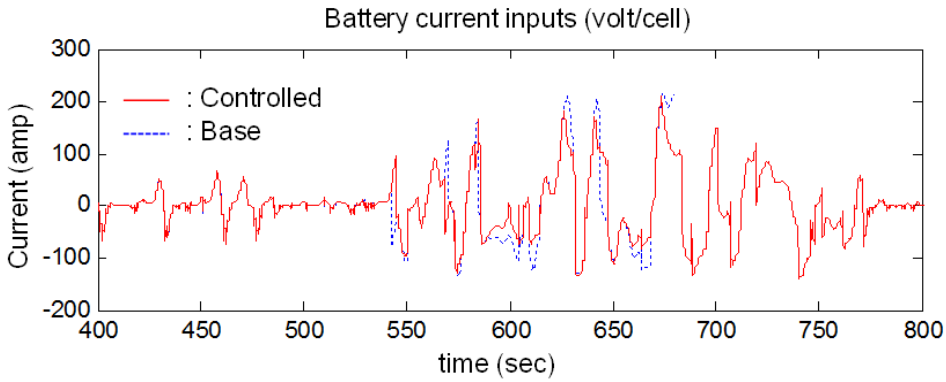


(b)

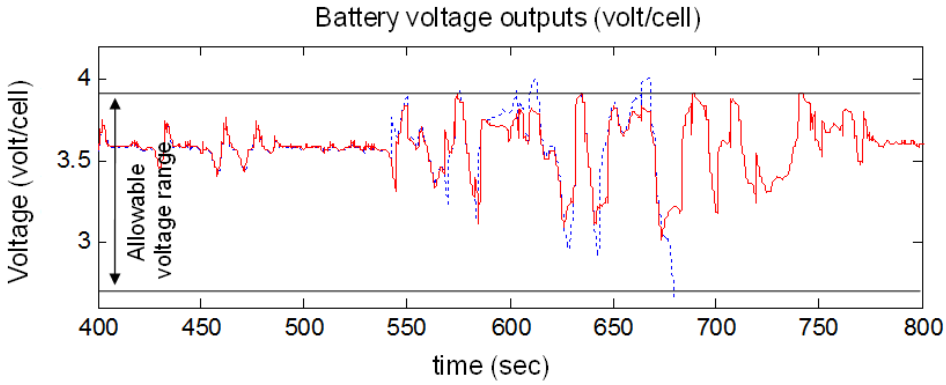


(c)

Fig. 9. Battery responses under transient by the proposed battery management strategy using the estimated Li-ion concentration by the EKF: (a) battery power limits; (b) battery current inputs; (c) battery voltage outputs

Simulation results with two different supervisory controls are shown in Fig 9. To illustrate the performance of the proposed control design, the simulation results within the most aggressive section are highlighted here. During sudden acceleration and deceleration, the magnitudes of power limits constrained as shown in Fig. 9 (a). The large adjustments occur around 680 seconds under severe acceleration. Li-ion concentration in the cathode increases suddenly. The base control strategy requires power computed without consideration of the Li-ion concentration, yet, the battery dynamics lead to a severe drop of the Li-ion concentration at the solid surface. Hence, further voltage drops occur, and the battery will be damaged by over-discharging. In contrast, the EKF captures the dynamic behavior and significantly modifies the instantaneous allowable power limits to maintain the battery terminal voltage within the safe limits.

The battery current inputs and voltage outputs are compared in Fig. 9 (b). Under the mild driving from 400 to 540 seconds, battery responses are exactly same each other with both control strategies. Under aggressive driving, the proposed controller limits the battery power demand to prevent further discharging and charging. Thus, the voltage range is kept within the allowable range.

Figure 9 (c) shows the comparison of the voltage traces between the base control and the proposed control. Without the battery power limit adjustment, the voltage fluctuation range is large and often beyond the battery operation range (2.7V~3.9V). The voltage exceeds the upper bound several times due to excessive regeneration braking. Under the severe acceleration, the uncontrolled battery current inputs result in severe voltage drops, then the battery finally cannot handle the power demand. In contrast, the controlled battery power limits allow the safe battery operation within the battery operating voltage range under fast transient.

## VI. CONCLUSIONS

This paper proposes a control strategy for the management of the allowable battery power limits to prevent excessive battery charging and discharging rates. First, the simulation framework for a series-HEV is constructed with the rule-based supervisory controller. The series-HEV simulation framework includes a finely discretized electrode-averaged electrochemistry battery model to capture the realistic battery voltage drops with respect to applied current. Then, a control strategy considering the dynamics of Li-ion diffusion is proposed to moderate excessive battery charging and discharging. The proposed controller modifies the allowable battery power limits by using the entire battery Li-ion concentration information along the solid particle. The rule-based supervisory controller uses the modified battery power limits and distributes the required power between the engine and the battery. The proposed control design uses the same rule-based supervisory controller structure, and it adjusts only the allowable battery power limits in the control rules. Thus, the overall supervisory controller complexity is not increased.

The battery Li-ion concentration profiles used in the control design is estimated by the electrochemical model-driven extended Kalman filter (EKF). The EKF is designed using the electrode-averaged electrochemistry model with uneven discretization of the particle radius for the fast and accurate prediction of the Lithium intercalation dynamics. The EKF shows good Li-ion concentration estimating performance over transient driving. Then, the allowable battery power limits are modified through the proportional-integral (PI) feedback of the weighted average of the Li-ion concentration difference from the bulk Li-ion concentration. The proposed battery power management strategy successfully prevents over-charging and over-discharging under aggressive driving. With the proposed battery control, smaller batteries can be used to obtain the same level of HEV performance and fuel economy while preventing battery degradation. Thus, the battery cost will be significantly reduced.

## ACKNOWLEDGEMENT

This work has been partially supported by the Automotive Research Center (ARC), a U.S. Army center of excellence in modeling and simulation of ground vehicles funded by TARDEC, Warren. Such support does not constitute and endorsement by the sponsor of the opinions expressed in this article.

## REFERENCES

[1] M. Doyle, T. Fuller, and J. Newman, "Modeling of galvanostatic charge and discharge of the lithium/polymer/insertion cell," *J. Electrochemical Society*, vol. 140, no. 6, pp. 1526-1533, 1993.

[2] T. F. Fuller, M. Doyle, and J. Newman, "Simulation and optimization of the dual lithium ion insertion cell," *J. Electrochemical Society*, vol. 141, no. 1, pp. 1-10, 1994.

[3] W. B. Gu, and C. Y. Wang, "Thermal and electrochemical coupled modeling of a lithium-ion cell", *Proc. ECS*, 2000.

[4] Smith, K. A., Rahn, C. D., and Wang, C. Y., "Model order reduction of 1D diffusion systems via residue grouping", J. Dynamic Systems, Measurement and Control, vol. 130, pp. 011012.1-011012.8, 2008.

[5] Smith, K. A., Rahn, C. D., and Wang, C. Y., "Model-based electrochemical estimation and constraint management for pulse operation of Lithium ion batteries", IEEE Trans. Control system Technology, vol. 18, no. 3, pp. 654-663, 2010.

[6] D. Di Domenico, G. Fiengo, and A. Stefanopoulou, "Lithium-ion battery state of charge estimation with a Kalman filter based on a electrochemical model," *Proc. 2008 IEEE Conf. Control Applications*, vol. 1, pp.702 – 707, 2008.

[7] D. Di Domenico, A. Stefanopoulou, and G. Fiengo, "Reduced order lithium-ion battery electrochemical model and extended Kalman filter state of charge estimation," *ASME J. Dynamic Systems, Measurement and Control - Special Issue on Physical System Modeling*, 2010.

[8] R. Patil, B. Adornato, and Z. Filipi, "Design Optimization of a Series Plug-In Hybrid Electric Vehicle for Real-World Driving Conditions," SAE Technical Paper No. 2010-01-0840, 2010.

[9] P. Sharer, A. Rousseau, S. Pagerit, and P. Nelson, "Midsize and SUV vehicle results for plug-in HEV component requirements," SAE Technical Paper No. 2007-01-0295, 2007.

[10] Z. Filipi, and Y. J. Kim, "Hydraulic hybrid propulsion for heavy vehicles: combining the simulation and engine-in-the-loop techniques to maximize the fuel economy and emission benefits," *Oil & Gas Science and Technology*, vol. 65. No. 1, pp. 155-178, 2009.